

Fault-tolerant High-power Two-phase Coreless AFPM Motor-drive System Concept

Yaser Chulaee, *Senior Member, IEEE*, Ali Mohammadi, *Member, IEEE*,
Matin Vatani, *Graduate Student Member*, Aaron Cramer, *Senior Member, IEEE*, Dan M. Ionel, *Fellow, IEEE*

Abstract—This paper proposes a fault-tolerant, high-power two-phase coreless axial flux permanent magnet (AFPM) motor-drive system concept. Initially, the performance of a two-phase variant of the coreless AFPM machine is compared with that of its three-phase counterpart using both 3D finite element analysis (FEA) and experiments. Thanks to the intrinsic unique features of coreless AFPM machines, the analysis of the results demonstrates that the two-phase configuration has comparable power density (kW/kg) and efficiency. In terms of fault tolerance, the two-phase configuration exhibits superior performance, as the mutual inductance between phases is zero, resulting in an electric machine with magnetically decoupled phases. Hence, the adverse effects of stator winding faults in one phase do not propagate to another. The proposed two-phase motor-drive system concept was demonstrated with a coreless AFPM machine featuring a modular printed circuit board (PCB) stator. The normal and post-fault operation of this machine was experimentally evaluated with a two-phase SiC-based control system with a high switching frequency to reduce current ripple due to the ultra-low phase inductance in coreless machines. Results demonstrated that, thanks to the magnetically and electrically isolated phases of the proposed motor-drive system, the machine can still operate after isolating the faulty phase using the controller.

Index Terms—Axial-flux, coreless machines, FEA, permanent-magnet machines, PCB stator, drive-systems, field oriented control, square-wave control, wide bandgap semiconductors.

I. INTRODUCTION

Permanent magnet synchronous machines (PMSMs), particularly those of axial flux type are being researched and developed for various applications, such as HVAC systems, industrial motor-drives, aviation propulsion, and electric vehicles [1]. Stator coreless axial flux permanent magnet (AFPM) machines offer unique advantages over conventional cored electric machines. Within coreless machines, due to the lack of a magnetic core and its associated power losses, there is potential to achieve high efficiency and power density. In the absence of stator teeth, these machines do not experience cogging torque, resulting in a very smooth output torque profile and low acoustic noise [2], [3].

Lack of a magnetic core can lead to potentially lower weight and volume, depending on the application and system integration. Eliminating the magnetic core allows for more effective cooling systems, wherein the coolant can be in direct contact with the stator windings within liquid-cooled motors, enabling the opportunity to increase current density multiple times that of a conventional cored machine [4], [5]. This can potentially improve power density and specific torque (Nm/kg). These features collectively make coreless machines well-suited for those applications demanding high speed and

power density, including electric aircraft propulsion systems and electric vehicles [2].

Axial flux PM machines incorporating coreless stators exhibit ultra-low phase inductance (per unit value) due to a wide magnetic airgap. This results in excellent dynamic response but also presents some control challenges [6]. The low phase inductance causes high current ripple when the machine is fed by a voltage source inverter (VSI), leading to additional power losses in the stator windings and rotor back-iron, as well as torque ripple [7]. Low phase inductance also limits the flux-weakening capability of the machine meaning the output power decreases faster above the rated speed compared to cored machines, resulting in a narrower speed range [1]. Therefore, to fully leverage the distinctive features of coreless machines and unleash their full potential, special measures must be taken in the control system design to prevent degradation in machine performance.

A primary concern regarding PM machines, particularly in safety-critical applications such as electric aircraft propulsion systems, is their fault tolerance due to the inability to be de-excited, especially when connected to the loads with high inertia. Extensive efforts have been undertaken by the researchers to address this concern, focusing on both the machine itself and its control system. This includes implementing corrective control strategies for power converters.

Lack of the stator magnetic core in coreless machines creates an opportunity to incorporate printed circuit board (PCB) stators into coreless AFPM machines. Printed circuit board stators have gained popularity due to their flexibility in designing the coil shape, potentially reliable and highly repeatable fabrication process, as well as their lightweight design [8]–[10]. Moreover, PCB stators enable a modular design, leading to ease of maintenance, improved reliability, and cost efficiency. The modular design facilitates the creation of AFPM machines with a different number of phases by effortlessly stacking PCB stators without any major changes in the machine's geometry [11], [12].

This paper is a follow-up expansion of [13] and [14] and proposes a fault-tolerant high-power two-phase modular PCB stator coreless AFPM motor-drive system offering comparable power density and efficiency to its three-phase counterpart. Although PCB stator coreless machines presented in the literature are typically fractional-horsepower, rated below 1 kW, and designed for limited applications, such as those described in [15], this paper introduces an integral-horsepower PCB stator coreless AFPM motor-drive system that delivers 12 N·m at

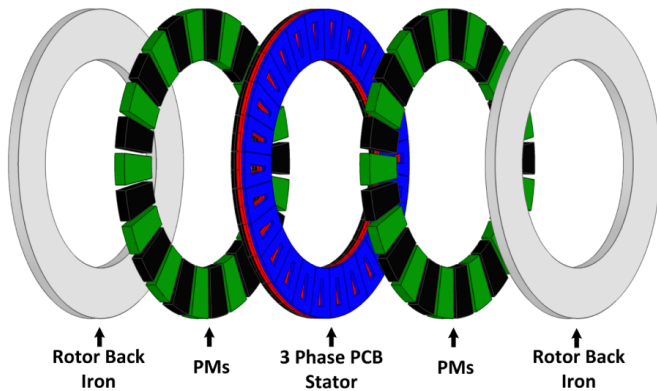


Fig. 1. The exploded view of the example double-rotor coreless AFPM machine with modular PCB stator, where each PCB is dedicated to one phase.

1800 rpm with natural cooling and can be seamlessly scaled to higher power ratings.

Due to the unique intrinsic features of coreless AFPM machines, the introduced machine provides electrically insulated and magnetically decoupled phases, preventing fault propagation from one phase to another, thus offering a high level of fault tolerance for safety-critical applications. Initially, the performance of the proposed two-phase machine is compared with its three-phase counterpart from various perspectives using 3D finite element analysis (FEA) developed in Ansys Electronics Desktop, utilizing the transient solution type [1], [16]. The comparison study covers multiple aspects, including the magnetic circuit, efficiency, power losses, torque and power density, torque ripple, design challenges, and control systems, providing a comprehensive understanding of the distinctions between these motors. The accuracy of the models and FEA results was experimentally verified with the available prototype machine in the laboratory.

The proposed control system incorporates two operating modes: sine-wave and square-wave, designed for ultra-low inductance and high-polarity coreless AFPM machines. The square-wave control mode effectively extends the speed range by eliminating the reliance on precise position sensors at high speeds, offering the opportunity to employ sensorless control schemes or Hall effect sensors. The square-wave control fully utilizes the inverter DC-link voltage, further improving the achievable speed range. To reduce current ripple due to low phase inductance, the introduced control approach is implemented on an inverter with a high switching frequency, employing wide-bandgap semiconductor devices. The machine's performance under both control modes and fault conditions was experimentally studied and validated on a developed prototype PCB stator coreless AFPM machine and drive system.

II. TECHNOLOGY REVIEW

To maintain the current ripple within acceptable levels, low inductance motor drives typically necessitate a switching frequency in the range of 50–100 kHz [6]. In conventional drive systems for low inductance machines, current ripple and

PWM reflected current harmonics are reduced by using LC and LCL filters. A drawback in LC filters is that they can cause distortion in voltage and current waveforms, particularly in the LC resonant range, and can result in circulating currents between the inverter and the filter. Additionally, LCL filters can lead to increased system cost, weight, and volume [7]. The authors in [17] tackle these challenges by combining the PCB motor with wide-bandgap devices (GaN FETs) and increasing the switching frequency to the megahertz range. This approach helps to reduce current ripple and minimize the size of the filtering components. The study evaluates different filtering options and ultimately selects an L filter with line inductors for the motor phases.

To expand the flux weakening region of low-inductance machines, it is necessary to fully utilize the VSI DC-link. Additionally, certain modifications should be made to the machine design, if possible. An integrated stator-embedded inductor was proposed in [18] to improve the field-weakening operation of low-inductance slotless PMSMs. This approach also mitigates PWM-induced current ripple and associated losses. To overcome the lack of an inverter voltage source above the base speed in conventional drive systems for high-speed applications, z-source inverters with voltage-boost capability were introduced in [19]. Z-source converters are capable of providing flexible voltage gain and improving system reliability [20]. Applying square-wave voltage to machine terminals or using over-modulation at high speeds is another technique to fully utilize the inverter DC-link and push the speed limit. A new current regulator, capable of providing a wider operating range for PMSMs operating in square-wave mode at high speeds, was proposed in [21] for rail traction systems.

The combinations of slot and pole numbers that force the coupling between phases to be essentially zero have been previously investigated in [22]. This ensures that a fault in one phase does not adversely affect the remaining healthy phases, leading to improvements in fault tolerance. Practical combinations of slot and pole numbers for fault-tolerant permanent magnet brushless machines operating in multiplexed 2-phase and 3-phase configurations have been determined in [23]. A comprehensive literature review of proposed methods for improving fault tolerance in PM synchronous machines was presented in [24].

III. TWO- AND THREE-PHASE CORELESS AFPM MACHINES WITH COMPARABLE DIMENSIONS AND PERFORMANCE

In this research, the example coreless AFPM machine under study is a 36-pole, integral horsepower, double-rotor machine with a PCB stator. This machine consists of separate PCB stators, one for each phase, with 36 spiral-shaped coils placed between two PM rotors, which are made of NdFeB magnets with a grade of N52. The double-rotor, single-stator configuration, as shown in Fig. 1, is commonly chosen for its high torque and power densities and robustness [25].

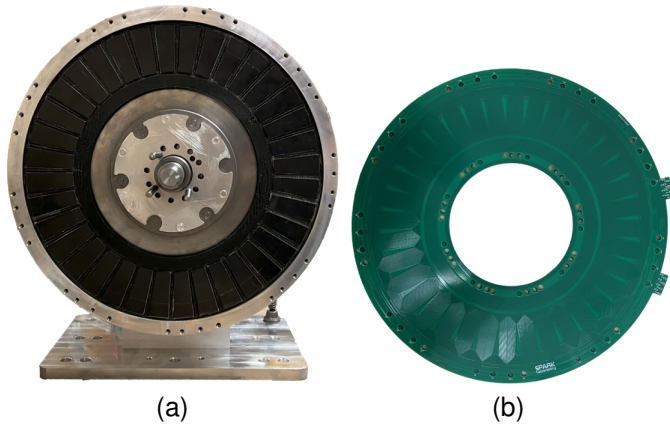


Fig. 2. The rotor magnets (a) and the fabricated two-phase PCB stator (b) of the under study prototype coreless axial flux permanent magnet machine.

TABLE I
SPECIFICATIONS AND MAIN DIMENSIONS OF THE EXAMPLE PROTOTYPE MACHINE FOR THIS STUDY.

Parameter	Value	Unit
No. of poles	36	-
Rated torque	12.0	N.m
Rated speed	1,800	rpm
Torque constant	2.1	N.m/A
Torque density (natural cooling)	6.6	N.m/L
Airgap (per side, magnet to stator)	1.3	mm
Stator thickness (three-phase)	6.0	mm
Rotor inner/outer diameter	208/304	mm
Stator inner/outer diameter	202/310	mm
Inertia	4.22	kg · m ²
PM type	NdFeB (N52)	-

Coreless stators can be designed with either conventional concentrated or distributed windings using Litz wires or PCB technologies. Within conventional stator windings, distinct phase windings are placed on a common plane, with mechanical shifts equivalent of 72, 90, 120, and so forth, electrical degrees relative to each other, contingent upon the number of phases. Hence, to modify the number of phases, the stator needs to be redesigned, involving changes from alteration of the coil shape to wiring.

The under study example prototype PCB stator AFPM machine is shown in Fig. 2. The detailed design and prototyping process are discussed in another research paper by the same group of authors [26]. The modular design, where each independent PCB is dedicated to one phase, facilitates the creation of AFPM machines with different numbers of phases by stacking stators. For example, a three-phase machine can be assembled by shifting three PCB stators by 120 electrical degrees (e.g., 6.66 mechanical degrees for this 36 pole machine) with respect to each other and then stacking them together. The machine specifications, and main dimensions are presented in Table I.

In the following, the performance of a two-phase variant of the introduced PCB stator coreless AFPM machine is compared with its three-phase counterpart. This comparison

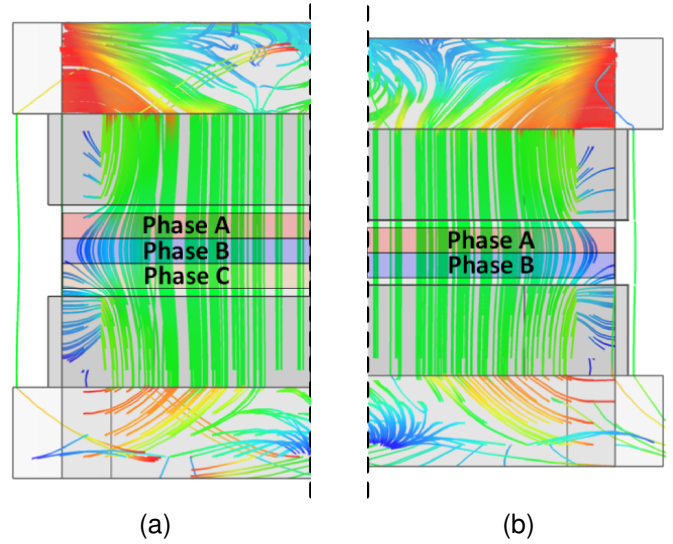


Fig. 3. Cross-sectional view of the introduced three-phase (a) and two-phase (b) PCB stator machines. The mechanical airgap, i.e., the distance between the magnet and PCB surfaces, is the same for both configurations. The two-phase configuration is marginally shorter by one PCB, which is equivalent to 2mm.

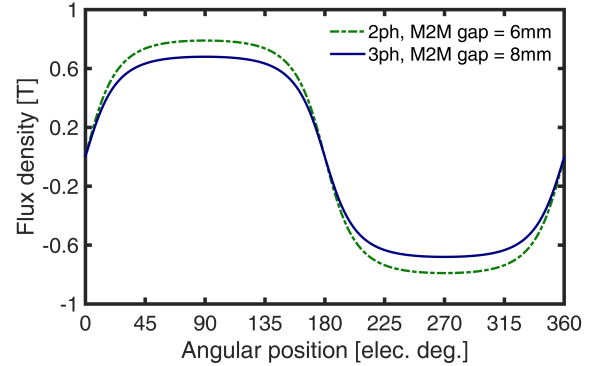


Fig. 4. The airgap flux density of the machines under study based on FEA. The fundamental component of the airgap flux density is approximately 16% higher in the two phase machine due to the smaller magnet to magnet (M2M) gap.

is carried out using the developed FEA models for both configurations, as well as through experiments. The cross-sectional views of the developed 3D FEA models for the three-phase and two-phase coreless AFPM machines are shown in Fig. 3. Each PCB stator has a thickness of 2mm, and the mechanical airgap, i.e., the distance between the rotor magnets and the PCB surface, is kept constant at 1mm for both configurations.

For a double-rotor non-salient AFPM machine, the fundamental of the torque producing components of the airgap flux density, $B_{z,1}$, can be represented as [25]:

$$B_{z,1}(\theta, z) = \hat{B} \cosh\left(\frac{\pi}{\tau_p} z\right) \cos(\theta), \quad (1)$$

with the peak value:

$$\hat{B} = \frac{4B_r}{\pi} \frac{\sinh[\pi(k_\sigma k_b h_m / \tau_p)]}{\sinh[\pi(k_c g / 2\tau_p)]} \sin\left(\frac{\pi}{2} k_m\right), \quad (2)$$

where B_r is the remanence of the PMs, τ_p the pole pitch, h_m the magnet thickness, g the airgap length, and $k_m = \tau_m / \tau_p$ the pole-arc to pole-pitch ratio. The dimensions of the magnets, i.e., thickness, h_m , and arc length, τ_m , for a target airgap flux density and a specified magnet type can be decided [27]. Carter's and PM leakage coefficients are represented by k_σ and k_c , respectively. Both can be approximated with a unity value for surface PM (SPM) coreless machines. The coefficient k_b is equal to the number of PMs that provide the polar flux with a unity value for SPM.

In the example design, eliminating one phase (i.e., one PCB stator) allows us to reduce the magnetic gap by 2 mm. Consequently, based on equation (2) and the analytical calculations, the two-phase motor exemplified on the right side of Fig. 3 exhibits an approximately 16% higher fundamental component of the airgap flux density compared to the three-phase machine, as depicted in Fig. 4, derived from finite element analysis. This is due to the unique intrinsic feature of stator coreless machines and cannot be replicated by cored machines.

The electromagnetic torque of a PM synchronous machine can be estimated by:

$$T_{em} = \frac{m}{2} p \Psi_{PM} J_{rms} SFF c_w \ell_c / N_t, \quad (3)$$

where m is the number of phases, p the number of pole pairs, Ψ_{PM} airgap flux density generated by rotor PMs, J_{rms} the current density in copper conductors, c_w the coil side width, ℓ_c the coil axial thickness, and SFF the slot-fill-factor.

Hence, according to equations (2) and (3), the two-phase machine delivers approximately 28% lower torque compared to the three-phase machine, while maintaining the same envelope (the two-phase machine is only 2mm thinner in the axial direction). It is important to emphasize that, in a cored axial or radial machine, removing one phase results in a torque reduction of at least 50%, which highlights a significant advantage of coreless AFPM machines, making them an ideal candidate for a two-phase fault-tolerant design with a comparable performance. In order to facilitate a fair comparison, the two-phase and three-phase machines need to be assessed while delivering the same torque and power. Consequently, the phase current of the two-phase machine needs to be increased to compensate the torque drop.

The accuracy of the developed 3D finite element analysis models for both two-phase and three-phase prototype machines is verified by comparing the FE-based calculated back-EMFs with the experimentally measured ones. As shown in Fig. 5, there is very good agreement between the FEA results and the measurements.

It should be noted that Joule losses are not the only loss component within the stator windings. Coreless AFPM machines are subject to potentially high eddy and circulating current losses due to a lack of protection of stator teeth

TABLE II
THE EXPERIMENTALLY MEASURED POWER LOSSES AND PERFORMANCE INDICES OF THE MACHINES UNDER STUDY WHILE DELIVERING THE SAME OUTPUT TORQUE OF 12NM AT THE RATED SPEED OF 1,800RPM. PHASE RESISTANCE IS IDENTICAL FOR BOTH CONFIGURATIONS, 0.57 Ω .

Parameter	2ph	3ph	Unit
Rated phase current	7.5	5.5	A,rms
Joule losses	64.4	51.6	W
Eddy current losses	14.9	16.6	W
Circ. current losses	≤ 1	≤ 1	W
Mechanical losses	22.3	22.3	W
Efficiency	95.7	96.1	%
Goodness	1.19	1.26	Nm/ $\sqrt{W_{Loss}}$

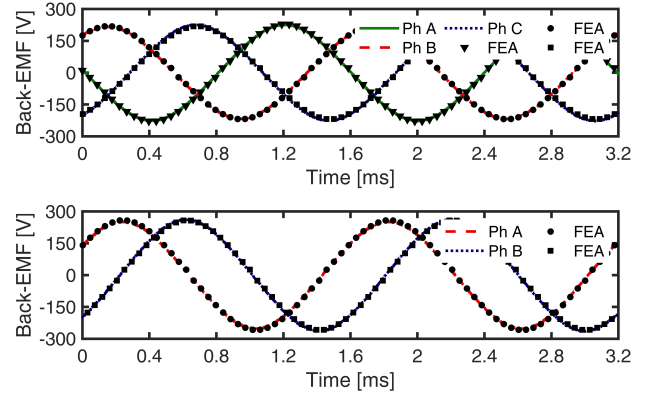


Fig. 5. Three-phase and two-phase back-EMFs of the prototype machines calculated by FEA and experimental tests.

[28]. Therefore, efficiency and goodness, $T_{em}g / \sqrt{W_{Loss}}$, are better performance indices to compare two-phase and three-phase configurations. The loss components in the coreless AFPM machine prototype using two and three-phase stators were experimentally measured and separated at the rated condition. The loss separations and phase currents of both three-phase and two-phase configurations, while delivering equivalent output power, as tabulated in Table II, enable a comprehensive comparison of the machines under study.

A smaller magnet-to-magnet gap in the two-phase configuration leads to a higher back-EMF. From a control system perspective, to maintain the back-EMF at a constant level and avoid the need to modify the inverter DC-Link (approximately a 15% increase for the example machine under study), the number of turns per phase can be slightly adjusted. By doing so, the voltage ratings of the switches used in the inverter for the two-phase machine will be the same as those for the three-phase machine inverter.

The phase currents of the two-phase example coreless AFPM machine are approximately 35% higher compared to the three-phase variant, and this must be considered in the selection of the inverter power switches and the design of its cooling system. The analysis of the results shows that the two-phase and three-phase configurations have comparable specific power (kW/kg) and efficiency. Within this example study, when both machines are delivering 12Nm at 1800rpm (2.26kW), the three-phase machine has only about a half-point

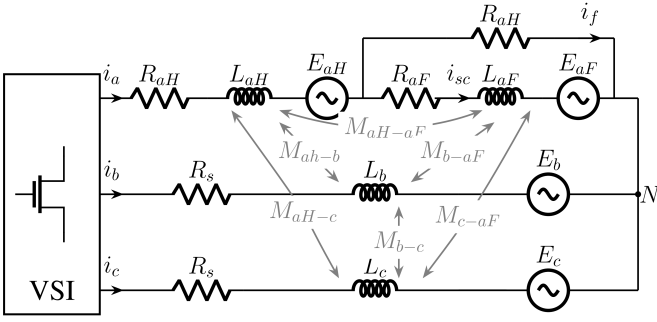


Fig. 6. Equivalent circuit model of a three-phase PMSM with an ITSC in phase A.

higher efficiency.

To develop an effective motor cooling system, it is imperative to take into account the total power losses. Comparative analysis indicated that the overall stator losses of the three-phase configuration is 16%. It is crucial to highlight that heat dissipation occurs on the surfaces of the PCBs. Consequently, despite the slightly higher losses within the two-phase machine which results in a higher temperature rise, both machines' stators share the same surface area, and their cooling systems can be identical.

It is worth mentioning that the introduced two-phase coreless machine design, which offers comparable power density and performance to its three-phase counterpart, can be achieved by effortlessly reconfiguring modular PCB stators without any changes to the stator or rotor structure and design. This is not possible with cored axial and radial flux machines. In a cored machine, apart from the need for major winding reconfiguration to form a two-phase machine, the input phase current must be increased by more than 50% to compensate for the torque drop due to eliminating one phase. This is dependent on saturation effects in the core, which results in higher losses. In fact, unlike a coreless machine, eliminating one phase in a cored machine does not provide any performance benefits, such as enhancing airgap flux density.

IV. FAULT TOLERANCE

Mutual inductance plays a significant role in the propagation and severity of faults in the stator windings. It represents the coupling between phases, which is a critical factor in determining the machine's post-fault operation. Post-fault operation is always challenging because a fault in one phase can propagate to another phase through mutual inductance.

One of the most common types of faults in the stator windings is an inter-turn short circuit (ITSC) fault within a single phase. An equivalent circuit model of a three-phase star-connected PMSM machine with an ITSC fault in phase A is shown in Fig. 6. The phase voltage equations in the presence of this fault are given in (4), indicating that the short-circuit fault, i_{sc} , impacts the currents and voltages of the other phases through mutual inductances, M [29].

TABLE III
THE MEASURED SELF AND MUTUAL INDUCTANCES FOR THE UNDER STUDY TWO- AND THREE-PHASE MACHINES. THE PER UNIT VALUE OF THE MEASURED PHASE RESISTANCE IS 0.018.

Configuration	L_{aa} [μH]	L_{ab} [μH]	L_{aa} [p.u.]	L_{ab} [p.u.]
Two Phase	33.4	0.0	0.0034	0.0
Three Phase	32.3	11.6	0.0033	0.0012

$$\begin{aligned}
 \begin{bmatrix} V_{aN} \\ V_{bN} \\ V_{cN} \\ 0 \end{bmatrix} &= \begin{bmatrix} r_s & 0 & 0 & -r_{af} \\ 0 & r_s & 0 & 0 \\ 0 & 0 & r_s & 0 \\ r_{af} & 0 & 0 & -r_{af} - r_f \end{bmatrix} \begin{bmatrix} i_a \\ i_b \\ i_c \\ i_{sc} \end{bmatrix} \\
 &+ \begin{bmatrix} L_{ah} & M_{ah-b} & M_{ah-c} & M_{ah-af} \\ M_{ah-b} & L_b & M_{b-c} & M_{b-af} \\ M_{ah-c} & M_{b-c} & L_c & M_{c-af} \\ M_{ah-af} & M_{b-af} & M_{c-af} & L_{af} \end{bmatrix} \\
 &\times \frac{d}{dx} \begin{bmatrix} i_a \\ i_b \\ i_c \\ i_{sc} \end{bmatrix} + \begin{bmatrix} e_{ah} \\ e_b \\ e_c \\ e_{af} \end{bmatrix}. \quad (4)
 \end{aligned}$$

In the previous section, the performance of a two-phase coreless AFPM machine was compared with that of its three-phase counterpart. The results indicated that the two-phase machine has comparable performance in terms of torque, power density, and efficiency. However, in terms of fault tolerance, it outperforms the three-phase configuration due to its zero mutual inductance.

The measured self and mutual inductances for both two-phase and three-phase prototype machines are reported in Table III. In a two-phase machine, the flux generated by a current in one phase winding does not link to the other phase winding, which is displaced by 90 electrical degrees in space. As a result, there are no mutual inductances. Hence, the machine phases are magnetically decoupled, and the adverse effects of a fault in one phase do not propagate to another.

In the modular PCB stator two-phase coreless AFPM machine introduced, each PCB stator is dedicated to a phase, providing very effective electrical insulation between the phases. One of the most common inverter topologies for controlling two-phase machines is shown in Fig. 7a, where each phase is connected to an independent single-phase inverter. This configuration adds two additional switches compared to a typical three-leg inverter, increasing cost but significantly enhancing electrical insulation and modularity. As the phases are magnetically and electrically decoupled, the faulty phase can be effortlessly isolated by the controller, ensuring post-fault operation as a single-phase machine.

To assess the machine's fault tolerance, its post-fault operation is studied both analytically and experimentally. The analytically calculated output torque waveforms of the two-phase machine are presented in Fig. 8, showing both the operational state when both phases are active and the faulted state when one phase is lost. If the faulty phase is isolated

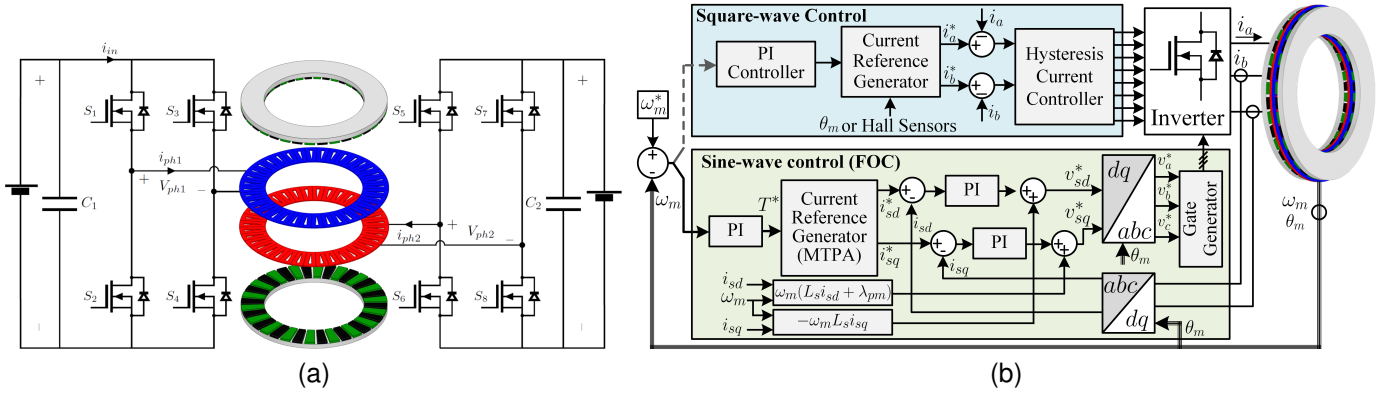


Fig. 7. Three-phase inverters connected to the PCB stators (a). The block diagram of the dual-mode drive system (b). Sine-wave and square-wave control modes are used interchangeably.

by the controller, the output torque exhibits pulsations with a consistently non-zero average, as shown in Fig. 8.

The substantial rotor inertia in axial flux machines, due to their narrow axial direction relative to their large outer diameter, acts as a mechanical filter (i.e., the rotor's angular acceleration becomes considerably less pronounced), effectively damping the negative impacts of these pulsating torques on the speed profile. As an example, the inertia of the prototype machine is $4.22 \text{ kg} \cdot \text{m}^2$, which is two orders of magnitude greater than that of a radial flux counterpart. The post-fault operation of the prototype is also experimentally investigated in the following sections.

Although the mutual phase inductance in a two-phase machine is zero and potential short-circuit fault currents in one phase do not propagate to the other, the impact of large transient short-circuit currents must still be considered. In conventional cored electric machines, one of the most critical effects of large fault currents is permanent magnet (PM) demagnetization. However, unlike in cored machines, armature reaction, as well as skin and proximity effects, are negligible in coreless machines due to the absence of stator teeth, as thoroughly studied in [26], [30]. Consequently, even large transient fault currents do not pose a risk of PM demagnetization.

In order to address the previously mentioned control challenges within coreless AFPM machines, a dual-mode drive system has been proposed. The control system features two modes: field-oriented control (FOC) and square-wave control, which can be switched depending on the machine's operational region and condition. To tackle the intrinsic challenge of controlling coreless machines—high current ripple due to ultra-low phase inductance—a high switching frequency of over 60kHz is used for the inverter, enabled by SiC MOSFETs. The following sections will discuss both operational modes and examine the potential advantages of the proposed control approach in enhancing the system's reliability and fault tolerance.

The machine's configuration and its connections to the two-phase inverter are shown in Fig. 7a. Each inverter leg uses one

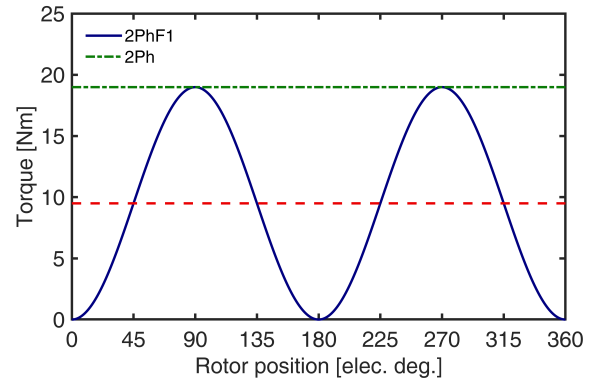


Fig. 8. The analytically calculated output torque waveforms of the example two phase machines when all phases are healthy (2Ph) and one phase is isolated by the controller due to a fault (2PhF1). The average values of the waveforms are plotted with dashed lines.

CREE silicon carbide (SiC) MOSFET evaluation kit. The kit includes two Cree 80mOhm, 1200V, 36A CREE MOSFETs (C2M0080120D) and two 1200V 20A Schottky diodes. It also features a half-bridge evaluation board equipped with isolated gate drivers, power supplies, and all the components necessary for the rapid assembly of the half-bridge power stage. SiC MOSFETs, recognized as wide bandgap semiconductor devices, offer the advantage of fast switching with low drain-source on-state resistance, resulting in relatively lower switching power losses compared to conventional semiconductor devices.

A. Field-Oriented Control (FOC)

Field-oriented control is a widely recognized technique for managing the output torque and speed of electric machines by regulating the currents in a rotational direct and quadrature (dq) reference frame. In this approach, the stator currents are transformed into flux-producing and torque-producing components, which are DC waveforms and can be independently regulated by conventional controllers, such as

proportional–integral–derivative (PID) controllers, to achieve specific objectives and commands.

In the surface-mounted AFPM machine under study, the rotor is non-salient, and the stator winding voltages in the dq reference frame are as follows:

$$\begin{aligned} v_{sd} &= R_s i_{sd} + \frac{d}{dt} \lambda_{sd} - \omega_s \lambda_{sq} ; \\ v_{sq} &= R_s i_{sq} + \frac{d}{dt} \lambda_{sq} + \omega_s \lambda_{sd} , \end{aligned} \quad (5)$$

where,

$$\lambda_{sd} = L_s i_{sd} + \lambda_{pm} ; \quad \lambda_{sq} = L_s i_{sq} , \quad (6)$$

and λ_{pm} is the rotor PMs flux linkage. In these equations, R_s is the stator winding resistance, and L_s represents the stator winding inductance, which consists of the stator winding leakage inductance, L_l , and magnetizing inductance, L_m . The synchronous speed is denoted by ω_s .

Based on the interaction between the stator current and the magnetic flux produced by the rotor PMs, the electromagnetic output torque can be expressed as:

$$T_{em} = \frac{m}{2} \frac{p}{2} (\lambda_{sd} i_{sq} - \lambda_{sq} i_{sd}), \quad (7)$$

where m and p are the number of phases and poles, respectively [31]. Substituting (6) into (7) leads to the following equation for a non-salient machine:

$$T_{em} = \frac{m}{2} \frac{p}{2} [(L_s i_{sd} + \lambda_{pm}) i_{sq} - L_s i_{sq} i_{sd}] = \frac{m}{2} \frac{p}{2} \lambda_{pm} i_{sq}. \quad (8)$$

Hence, the maximum torque per ampere (MTPA) control strategy for a non-salient pole PM machine when operating below the rated speed can be achieved by setting the d-axis current i_{sd} to zero (i.e. $\hat{I}_s = i_{sq}$).

A cascade control structure is often employed to regulate the torque-producing component of the stator current and to achieve the desired commands, such as torque or speed set points. In cascade control, the inner current loop should have a higher bandwidth than the outer loops. The high switching frequency achieved by WBG semiconductor devices can significantly improve the controller's bandwidth, leading to a high-performance and stable drive system.

The block diagram of the FOC-based speed control system for the AFPM machine under study is illustrated in Fig. 7b. In such control systems, proportional-integral (PI) controllers are typically used to minimize d-axis and q-axis current errors by generating appropriate reference stator voltages, which are then used to produce gate signals for the switches.

The initial assumption is that the d-axis and q-axis currents can be separately controlled by these controllers. However, there are coupling effects between them that may lead to performance degradation of the controllers. The commonly used feed-forward decoupling scheme addresses this issue by adding compensation terms (i.e., $\omega_m(L_s i_{sd} + \lambda_{pm})$ and $-\omega_m L_s i_{sq}$) to the stator voltage references, as shown in Fig. 7b.

To handle saturation and avoid large overshoots, torque and current limiters, as well as clamping anti-windup, were considered in the implementation of the PI controllers. The bipolar sinusoidal pulse width modulation (SPWM) technique is employed in this control scheme due to its lower complexity and computation time compared to the space vector modulation (SVM) method. The performance of the introduced machine under this control mode is experimentally investigated, and the results are provided in Section VI.

It is worth mentioning that, from a control theory perspective, there is no difference between the FOC-based drive system of a PM two-phase machine and that of a three-phase PM machine. However, certain implementation details must be considered. The generated voltage references, v_a^* and v_b^* , which are phase-shifted by 90 electrical degrees, are fed into separate single-phase inverters, as shown in Fig. 7a. These inverters can either share the same DC link or have separate DC links to enhance reliability. Since the phases are electrically separated, it is necessary to measure both phase currents to accurately compute the corresponding d and q axes currents.

For speeds higher than the rated speed, the induced voltage of the motor needs to be maintained at the rated voltage; otherwise, the control system may fail due to insufficient voltage. Therefore, a negative d-axis current, proportional to the increase in speed, is typically applied. This weakens the rotor magnetic field and, consequently, helps maintain a constant induced voltage. This method, known as flux-weakening, ensures constant power operation beyond the rated speed.

Within coreless machines, the phase inductance and armature reaction are not sufficiently large. Consequently, even at highly negative commands for i_{sd} , it is challenging to achieve effective flux weakening over a wide range of speeds. One effective approach to addressing this issue is a square-wave control scheme. This approach, which will be investigated in the following section, has the potential to extend the speed range of the machine by better utilizing the inverter's DC-link voltage.

B. Square-Wave Control

Square-wave control, also known as trapezoidal control, is a technique often used to operate brushless direct current (BLDC) machines with a trapezoidal-shaped back-EMF. The square-wave control can also be implemented in certain applications or operational regions for PMSM machines with sinusoidal back-EMFs [21]. A detailed explanation of this method, along with an advanced simulation model for BLDC motor drives and its actual implementation, is provided in [32].

Within this control method, phase commutations occur at specific rotor positions, which are typically determined by Hall effect sensors mounted on the stator windings. Hence, this control method offers straightforward implementation by eliminating the need for high-resolution position sensors and complex signal processing techniques. It should be noted that the Hall sensors arrangement should be properly modified

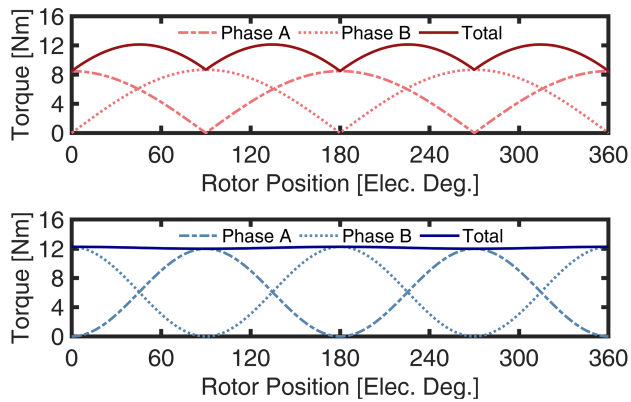


Fig. 9. The example torque waveforms for a two phase machine when excited by square-wave (top) and sine-wave (bottom) currents.

to capture phase commutation for a two-phase machine. The maximum achievable amplitude of the fundamental frequency component of an inverter output voltage with square-wave control approach is $V_{ph} = 4/\pi V_{dc}$, which is approximately 27% higher than that of a typical sinusoidal PWM. This enhancement will be reflected in the maximum achievable speed. In fact, better utilization of the DC-link is an effective technique for operating beyond the rated speed in low inductance coreless or slotless machines. The block diagram of the square-wave control scheme is demonstrated in Fig. 7b. In this method, the input quasi-square wave currents are typically regulated by a hysteresis controller to meet the commanded torque or speed [32].

It is important to note that, due to the absence of a magnetic core in air-cored machines, both armature reaction and proximity effects are negligible [26]. As a result, stator currents do not influence the airgap flux density. Consequently, the impact of square-wave current harmonics on eddy current losses in both the rotor magnets and the stator windings is minimal. In other words, PM flux density variations are the main source of eddy currents in the stator windings.

Apart from better utilization of the inverter DC link, square-wave control facilitates achieving ultra-high speeds with coreless machines. Unlike the FOC method, this approach does not require dq-abc transformations, advanced controllers, or complex PWM techniques, all of which are computationally demanding. Hence, square-wave control is a suitable choice for motor drives with very high switching frequencies. Within this approach, it is feasible to update the switching pattern at least once per switching period, even with low-cost processors.

Eliminating the need for high resolution encoders in the square-wave control enables an opportunity to employ low-cost solutions like Hall effect sensors that are more reliable in harsh environment [33], [34]. Lack of high-precision electromechanical encoders also removes another limitation to achieving ultra-high speeds. Sensorless control methods can also be employed to further simplify the hardware.

The main challenge of energizing AFPM machines with sinusoidal back-EMFs using square-wave currents is the torque ripple caused by the interaction between the square-wave

phase currents and sinusoidal back-EMFs. Examples of analytically calculated torque waveforms for a two-phase machine with sinusoidal back-EMF energized by square-wave and sine-wave input phase currents are compared in Fig. 9. The output torque of a coreless machine is theoretically ripple-free when a sine-wave current is applied, as there is no cogging torque. When square-wave currents are applied, the resulting torque waveform consists of segments of sine waves, which can potentially lead to noise and vibration.

The rotor of AFPM machines possesses high inertia due to its large diameter and relatively short stack length. High rotor inertia effectively attenuates the adverse effects of torque ripple caused by quasi-square wave current on the speed profile. In fact, the rotor's angular acceleration due to torque ripple is considerably reduced. The machine's performance under this condition is experimentally investigated in the following sections.

Depending on the application requirements, the nature of the load, and the operational region, the controller switches between these modes. Alternatively, based on the requirements, the machine can be controlled solely using one of these methods. For example, in an electric aircraft propulsion system, where the load has high inertia and there is a need for ultra-high-speed operation, high fault tolerance, and reliability, square-wave control can be employed across the entire operational region. Within this control method, there is no need for high-precision position sensors, and the control algorithm is straightforward, further improving the fault tolerance of the introduced motor-drive system.

V. EXPERIMENTAL RESULTS AND DISCUSSION

The performance of the proposed motor-drive system concept was evaluated through experiments on the prototype machine and test bench depicted in Fig. 10a. The prototype machine is coupled with an electronically controlled hysteresis brake as a controllable load. A non-contact torque sensor was placed between the prototype motor and the brake to measure the output torque. The machine is powered by a SiC-based inverter shown in Fig. 10b, which uses switch modules that were introduced previously. Hardware-in-the-loop (HiL) tests were conducted using the developed models in MATLAB/SIMULINK and dSPACE MicroLabBox to generate gate signals, perform real-time phase current and output torque measurements, interpret encoder data, and run the control algorithms.

The described field-oriented controller (speed control) was implemented to control the example two-phase machine under study, and its performance was evaluated through experimentation. The speed controller was meticulously designed, taking into account the mechanical system's time constant, to ensure stability during transient periods. The example two-phase motor-drive performance during a sudden change in load torque is shown in Fig. 11. The corresponding phase currents, which are nearly sinusoidal waveforms, and the dq-axis currents, shown in Fig. 12, exhibit negligible ripple, thanks to a high switching frequency of 65kHz. It can be inferred that

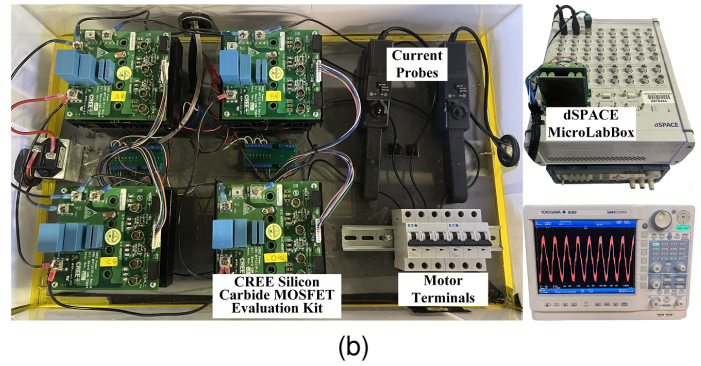
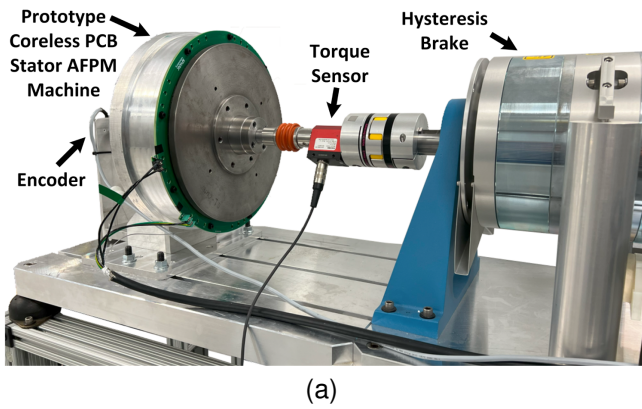


Fig. 10. The test bench for the example coreless AFPM machine used for this study. The machine is coupled with a controllable hysteresis break as a variable load (a). The inverter consists of CREE 1200V SiC MOSFET modules, and the dSPACE MicroLabBox is used for HiL tests (b).

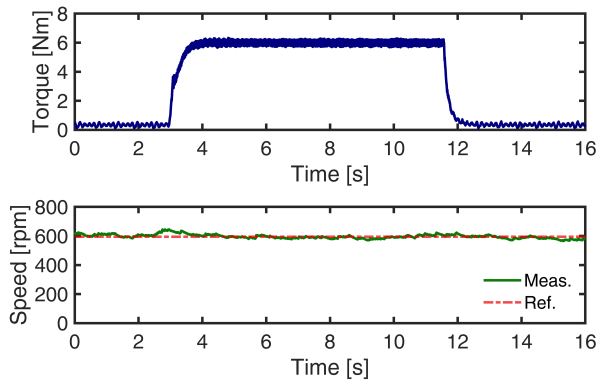


Fig. 11. Measured output torque and speed of the machine under study, controlled by the FOC method, during a sudden change in load applied by the hysteresis brake. The control system successfully maintained the speed at the commanded value.

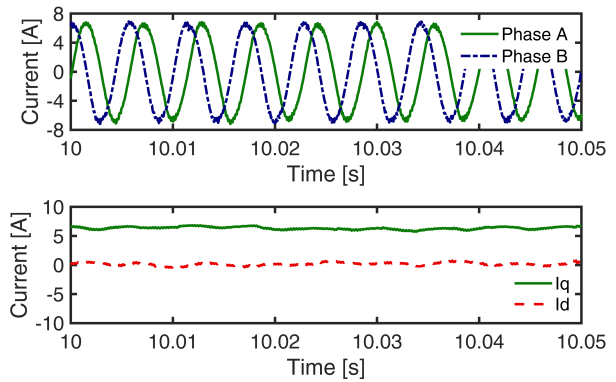


Fig. 12. A zoomed-in view of the measured two-phase and dq-axis current waveforms while the machine is controlled using the field-oriented method, with the torque profile shown in Fig. 11. The high switching frequency, thanks to the SiC-based inverter, resulted in nearly sinusoidal current waveforms with low ripple.

the two-phase machine delivers torque with low ripple while maintaining power density and efficiency comparable to the three-phase variant, along with a high level of electrical and magnetic isolation.

In the presence of high-frequency current harmonics even coreless machine may experience power losses in the rotor magnets and back-iron [7]. Experimental results have demonstrated that by employing a high switching frequency, the phase currents become nearly sinusoidal with low harmonic content.

The performance of the prototype machine when a single fault occurs was also investigated. A single-phase fault was emulated by isolating one phase through the control system. Torque ripple under this operating condition, where the machine is delivering 50% of the rated torque at 100rpm, is shown in the zoomed-in view of Fig. 13. The high number of poles results in smooth operation, even for the single-phase machine at low speeds. Although one phase is lost due to a fault, the machine can still deliver torque with reasonable ripple, with no significant increase compared to the healthy condition. The demonstrated speed profile is almost ripple-free and plateaued,

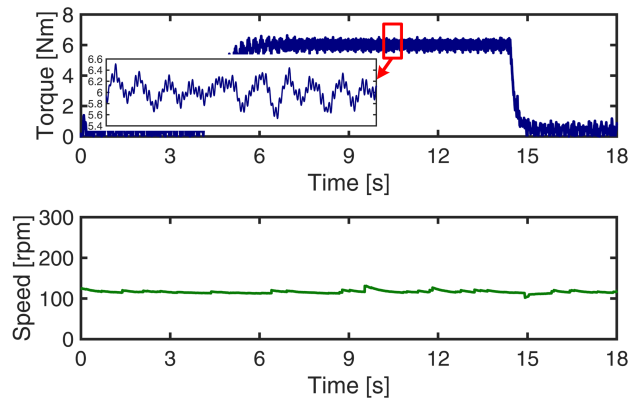


Fig. 13. Measured output torque and speed of the machine under study when one phase is isolated due to a fault. The zoomed-in view shows the torque ripple.

thanks to the high inertia of the rotor, even at relatively low speeds and with approximately 12% torque ripple.

The performance of the machine when it under the square-wave control mode was experimentally tested. The applied

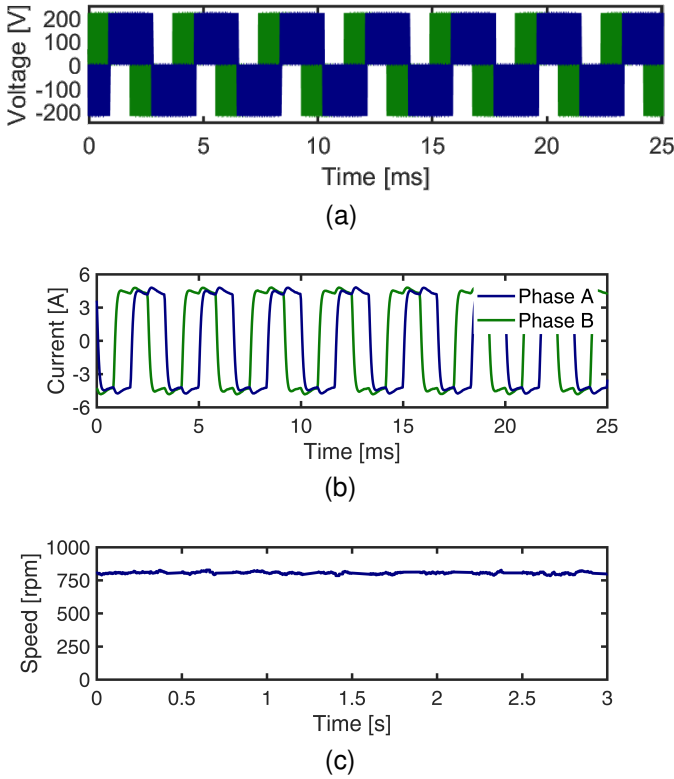


Fig. 14. Measured phase voltages (a), phase currents (b), and shaft speed (b) when the two-phase machine is operating under the square-wave control mode. The results show that the high rotor inertia effectively filters the negative impacts of high torque ripples induced by square-wave input currents on the speed profile.

two-phase square-wave currents are shown in Fig. 14b. The measured speed shown in Fig. 14c indicates that the prototype machine features a smooth speed profile even with square-wave phase currents, due to the effect of rotor inertia. High rotor inertia in AFPM machines can effectively dampen the negative impacts of torque ripple on the machine performance.

VI. DISCUSSIONS

The introduced coreless AFPM motor-drive systems have significant potential to further enhance power density and efficiency, making them a viable alternative to conventional electric machines in various applications. The absence of stator teeth provides direct access to the stator windings, enabling more efficient cooling. The implementation of advanced cooling systems, such as cooling pads [35] and cryogenic cooling, can significantly improve power density.

Although PCB stator coreless machines offer direct access to the windings, typical PCB substrate materials have relatively poor thermal conductivity. Therefore, studying and utilizing premium substrate materials with superior thermal conductivity, such as ceramic, could enhance stator cooling and provide an opportunity to further increase power density.

As discussed in this paper, high-switching-frequency voltage source inverters (VSIs) are required to minimize current ripple when controlling coreless machines. The use of Gallium

Nitride (GaN) switches enables ultra-high switching frequencies, further enhancing power density and efficiency [17].

The studied coreless AFPM machines are scalable to higher power ratings by stacking multiple rotors and stators. For instance, multi-disk coreless AFPM machines have been scaled to the megawatt level for electric aircraft propulsion systems, as discussed in [36].

The proposed coreless AFPM machine features modular PCB stators, where each phase is implemented on a separate PCB plane, mechanically shifted, and then stacked to form a distributed phase winding. In traditional implementations, stator coils for different phases share the same plane, creating a concentrated phase winding. While this arrangement may result in a thinner stator and a reduced magnetic circuit length (i.e., airgap), it also presents several disadvantages [37]. First, it lacks modularity, requiring a complete redesign of the PCB stator to accommodate different phase numbers. Additionally, it reduces electrical insulation between phases and increases maintenance costs, as individual faulty phases cannot be replaced separately.

Second, implementing effective techniques to mitigate circulating current losses, a common issue in coreless AFPM machines, becomes significantly more complex with this phase arrangement. For instance, the proposed layer transposition method described in [38] would be particularly challenging to integrate, especially in non-PCB stator designs. Therefore, the proposed modular design is strongly recommended for future coreless stator AFPM machines.

VII. CONCLUSION

This paper proposed a fault-tolerant, two-phase coreless axial flux permanent magnet (AFPM) motor-drive system concept. The concept was demonstrated through an integral horsepower modular PCB stator coreless AFPM machine. Analysis of the FEA and experimental results indicated that the introduced two-phase coreless AFPM machine had comparable power density and efficiency to that of its three-phase counterpart, thanks to its intrinsic unique features. The two-phase variant offered very high fault tolerance capability due to the magnetically decoupled and electrically insulated phases. With decoupled phases, the negative effects of a single-phase fault does not propagate to the other, ensuring post-fault operation.

The proposed drive system has two operational modes: field-oriented and square-wave. The square-wave control reduces computation time and eliminates the need for high-precision encoders, thus enhancing system reliability. Experimental results showed that the high torque ripple caused by quasi-square wave currents was dampened by the high rotor inertia in axial flux machines. The post-fault operation of the machine was also studied using the prototype, demonstrating that the machine was able to provide a non-zero average output after isolating one phase due to a fault. Thanks to the high rotor inertia, the rotor's angular acceleration becomes less pronounced, resulting in the single-phase machine producing a plateau-speed profile.

ACKNOWLEDGMENT

This paper is based upon work supported by the National Science Foundation (NSF) under Award No. #1809876. Any opinions, findings, and conclusions, or recommendations expressed in this material are those of the authors and do not necessarily reflect the views of the NSF. The support of Regal Rexnord Corp., Ansys Inc., and University of Kentucky, the L. Stanley Pigman Chair in Power Endowment is also gratefully acknowledged.

REFERENCES

- [1] M. Rosu, P. Zhou, D. Lin, D. Ionel, M. Popescu, F. Blaabjerg, V. Rallabandi, and D. Staton, "Multiphysics Simulation by Design for Electrical Machines, Power Electronics and Drives", J. Wiley - IEEE Press, 2017.
- [2] F. Nishanth, J. Van Verdegheem, and E. L. Severson, "A review of axial flux permanent magnet machine technology," *IEEE Transactions on Industry Applications*, vol. 59, no. 4, pp. 3920–3933, 2023.
- [3] V. Rallabandi, N. Taran, D. M. Ionel, and J. F. Eastham, "Coreless multidisc axial flux PM machine with carbon nanotube windings," *IEEE Transactions on Magnetics*, vol. 53, no. 6, pp. 1–4, 2017.
- [4] MachineDesign, "Axial flux motor topology signals next generation of electric motors," 2024. [Online]. Available: <https://www.machinedesign.com/mechanical-motion-systems/article/21281110/axial-flux-motor-topology-signals-next-generation-of-electric-motors>
- [5] P. Guedes-Pinto and R. A. Lee, "System, method and apparatus for direct liquid-cooled axial flux electric machine with PCB stator," U.S. Patent US11 482 908B1, 2021.
- [6] A. K. Morya, M. C. Gardner, B. Anvari, L. Liu, A. G. Yepes, J. Doval-Gandoy, and H. A. Toliyat, "Wide bandgap devices in AC electric drives: Opportunities and challenges," *IEEE Trans. on Transportation Electrification*, vol. 5, no. 1, pp. 3–20, 2019.
- [7] M. Leandro, N. Bianchi, M. Molinas, and R. B. Ummaneni, "Low inductance effects on electric drives using slotless permanent magnet motors: A framework for performance analysis," in *IEEE IEMDC 2019*, 2019, pp. 1099–1105.
- [8] F. Marcolini, G. De Donato, F. G. Capponi, and F. Caricchi, "Design of a printed circuit board axial flux permanent magnet machine for high speed applications," *IEEE Transactions on Industry Applications*, pp. 1–11, 2024.
- [9] Y. Chulaee, G. Heins, B. Robinson, M. Thiele, D. Patterson, and D. M. Ionel, "Design optimization considering a detailed PCB stator layout for coreless AFPM machines with minimal eddy and circulating current losses," in *2023 IEEE Energy Conversion Congress and Exposition (ECCE)*, 2023, pp. 3753–3758.
- [10] Y. Chulaee, D. Lewis, G. Heins, D. Patterson, and D. M. Ionel, "Winding losses in coreless axial flux PM machines with wave and spiral PCB stator topologies," in *2022 IEEE Energy Conversion Congress and Exposition (ECCE)*, 2022, pp. 1–6.
- [11] P. Han, D. Lawhorn, Y. Chulaee, D. Lewis, G. Heins, and D. M. Ionel, "Design optimization and experimental study of coreless axial-flux PM machines with wave winding PCB stators," in *2021 IEEE Energy Conversion Congress and Exposition (ECCE)*, 2021, pp. 4347–4352.
- [12] F. Marignetti, G. Volpe, S. M. Mirimani, and C. Cecati, "Electromagnetic design and modeling of a two-phase axial-flux printed circuit board motor," *IEEE Transactions on Industrial Electronics*, vol. 65, no. 1, pp. 67–76, 2018.
- [13] Y. Chulaee, A. Mohammadi, M. Vatani, and D. M. Ionel, "Fault-tolerant axial flux coreless PM machines with independent phase modules," in *2024 IEEE Transportation Electrification Conference and Expo (ITEC)*, 2024, pp. 1–5.
- [14] Y. Chulaee, A. Mohammadi, A. Cramer, and D. M. Ionel, "Flexible control for wide speed range operation of high polarity stator coreless AFPM machines with WBG semiconductor devices," in *2023 IEEE Energy Conversion Congress and Exposition (ECCE)*, 2023, pp. 4783–4788.
- [15] O. Taqavi and S. Mirimani, "Design aspects, winding arrangements and applications of printed circuit board motors: A comprehensive review," *IET Electric Power Applications*, vol. 14, pp. 1505–1518, 09 2020.
- [16] Ansys Electronics Desktop, Maxwell, version 23.1, 2023, ANSYS Inc.
- [17] O. Gulsuna, F. Tokgoz, F. Karakaya, and O. Keysan, "Design and analysis of a GaN-based megahertz integrated motor drive for a PCB motor," *IEEE Transactions on Industrial Electronics*, pp. 1–10, 2024.
- [18] M. S. Islam, R. Mikail, and I. Husain, "Field weakening operation of slotless permanent magnet machines using stator embedded inductor," *IEEE Transactions on Industry Applications*, vol. 57, no. 3, pp. 2387–2397, 2021.
- [19] O. Ellabban and H. Abu-Rub, "An overview for the z-source converter in motor drive applications," *Renewable and Sustainable Energy Reviews*, vol. 61, pp. 537–555, 2016.
- [20] S. Sharifi, Y. Chulaee, H. A. Zarchi, and M. Monfared, "Generalized three-winding switched-coupled-inductor impedance networks with highly flexible gain," *IEEE Transactions on Industrial Electronics*, vol. 68, no. 3, pp. 2130–2141, 2021.
- [21] D. Zhang, M. Zhou, C. Wang, and X. You, "A single-current-regulator flux-weakening control for PMSM under square-wave mode with wider operation range," *IEEE Transactions on Transportation Electrification*, vol. 8, no. 1, pp. 1063–1071, 2022.
- [22] A. Mitcham, "Favourable slot and pole number combinations for fault-tolerant PM machines," *IEE Proceedings - Electric Power Applications*, vol. 151, pp. 520–525(5), September 2004.
- [23] J. Chai, J. Wang, K. Atallah, and D. Howe, "Performance comparison and winding fault detection of duplex 2-phase and 3-phase fault-tolerant permanent magnet brushless machines," in *2007 IEEE Industry Applications Annual Meeting*, 2007, pp. 566–572.
- [24] A. M. EL-Refaie, "Fault-tolerant PM machines: A review," in *2009 IEEE International Electric Machines and Drives Conference*, 2009, pp. 1700–1709.
- [25] Y. Chulaee, D. Lewis, M. Vatani, J. F. Eashtam, and D. M. Ionel, "Torque and power capabilities of coreless axial flux machines with surface PMs and halfbach array rotors," in *2023 IEEE International Electric Machines and Drives Conference (IEMDC)*, 2023, pp. 1–6.
- [26] Y. Chulaee, G. Heins, B. Robinson, A. Mohammadi, M. Thiele, D. Patterson, and D. M. Ionel, "Design and optimization of high-efficiency coreless PCB stator axial flux PM machines with minimal eddy and circulating current losses," *IEEE Transactions on Industry Applications*, pp. 1–13, 2024.
- [27] D. Ionel, J. Eastham, T. Miller, and E. Demeter, "Design considerations for permanent magnet synchronous motors for flux weakening applications," *IEE Proceedings-Electric Power Applications*, vol. 145, no. 5, pp. 435–440, 1998.
- [28] Y. Chulaee, D. Lewis, A. Mohammadi, G. Heins, D. Patterson, and D. M. Ionel, "Circulating and eddy current losses in coreless axial flux PM machine stators with PCB windings," *IEEE Transactions on Industry Applications*, vol. 59, no. 4, pp. 4010–4020, 2023.
- [29] M. Zafarani, E. Bostanci, Y. Qi, T. Goktas, and B. Akin, "Interturn short-circuit faults in permanent magnet synchronous machines: An extended review and comprehensive analysis," *IEEE Journal of Emerging and Selected Topics in Power Electronics*, vol. 6, no. 4, pp. 2173–2191, 2018.
- [30] N. S., S. P. Nikam, S. Singh, S. Pal, A. K. Wankhede, and B. G. Fernandes, "High-speed coreless axial-flux permanent-magnet motor with printed circuit board winding," *IEEE Transactions on Industry Applications*, vol. 55, no. 2, pp. 1954–1962, 2019.
- [31] N. Mohan, "Electric Machines and Drives", J. Wiley, 2017.
- [32] B.-K. Lee and M. Ehsani, "Advanced simulation model for brushless DC motor drives," *Electric Power Components and Systems*, vol. 31, no. 9, pp. 841–868, 2003.
- [33] Y. Chulaee, H. A. Zarchi, and S. I. H. Sabzevari, "State estimation for sensorless control of BLDC machine with particle filter algorithm," in *2019 10th International Power Electronics, Drive Systems and Technologies Conference (PEDSTC)*, 2019, pp. 172–177.
- [34] J. Chen, X. Yuan, F. Blaabjerg, and C. H. T. Lee, "Overview of fundamental frequency sensorless algorithms for ac motors: A unified perspective," *IEEE Journal of Emerging and Selected Topics in Power Electronics*, vol. 11, no. 1, pp. 915–931, 2023.
- [35] D. D. Lewis, D. R. Stewart, M. Vatani, O. A. Badewa, A. Mohammadi, and D. M. Ionel, "Fault-tolerant topologies with halfbach array and PM-free multi-stage multi-module electric machines for electric aircraft propulsion," in *2024 IEEE Energy Conversion Congress and Exposition (ECCE)*, 2024, pp. 2524–2528.
- [36] M. Vatani, J. F. Eastham, and D. M. Ionel, "Multi-disk coreless axial flux permanent magnet synchronous motors with surface PM and halfbach

array rotors for electric aircraft propulsion,” in *2024 IEEE Energy Conversion Congress and Exposition (ECCE)*, 2024, pp. 4986–4992.

- [37] Y. Chulaee and D. M. Ionel, “Ultra-fast finite element analysis of coreless axial flux permanent magnet synchronous machines,” *IET Electric Power Applications*. [Online]. Available: <https://ietresearch.onlinelibrary.wiley.com/doi/abs/10.1049/elp2.12439>
- [38] Y. Chulaee, G. Heins, B. Robinson, A. Mohammadi, M. Thiele, D. Patterson, and D. M. Ionel, “Design and optimization of high-efficiency coreless PCB stator axial flux PM machines with minimal eddy and circulating current losses,” *IEEE Transactions on Industry Applications*, vol. 60, no. 6, pp. 8722–8735, 2024.